Method of manufactured solutions applied to variable-density flow solvers

By L. Shunn AND F. Ham

1. Motivation and objectives

The term *verification*, when applied to a flow solver, describes the process of demonstrating that the code correctly solves its governing mathematical equations. A code that has been properly verified, therefore, is in likelihood free of programming errors that affect the theoretical order-of-accuracy of the numerical algorithm. As such, code verification is an early and integral step in building confidence in the predictive capabilities of simulation software.

Over the past several decades, the complexity of computational algorithms in simulation codes has grown in response to demands for high-fidelity simulations in science and engineering. State-of-the-art simulation codes often involve complex exchanges of information amongst various physics modules, each of which may solve different equations using different algorithms on different grid topologies. As simulation codes become more sophisticated, thorough verification becomes increasingly challenging and time consuming, yet also more essential.

In this work, attention is focused on hydrodynamics codes amenable to low-Mach number combustion where acoustic effects are unimportant. In this framework, a variable-density formulation of the Navier-Stokes equations is often used due to its computational efficiency relative to fully compressible formulations. In the variable-density equations, the pressure and density are formally decoupled by defining the density through an equation-of-state (EOS) expressed in terms of transported scalars. The EOS may be given by an analytical expression, or as is common for complex reactive systems, it may be precomputed and tabulated as a function of the scalars.

Tabulated state-equations are heavily used in many popular combustion models. Examples include laminar flamelet models (Peters 1984, 2000), conditional moment closure (CMC) methods (Klimenko & Bilger 1999), and some transported PDF methods (Pope 1985). These combustion models are used in a variety of codes, targeting applications that include the design and optimization of engines and power systems, prediction of pollutant formation in combustion devices, and modeling and prediction of fires. While validation studies of combustion codes are routinely performed, the application of systematic verification studies is less common. In particular, the ramifications of tabulated state-relationships on the convergence and accuracy of combustion codes has not been widely investigated. As the EOS in typical combustion systems is multi-dimensional and highly non-linear, its implications on code performance are not straightforward.

Owing to the non-linear character of the governing equations, it is common to use iterative algorithms to solve the discretized system of equations. With these methods, solutions are iteratively refined from an initial guess until all equations are *approximately* satisfied at a given point and time. Iterative approaches, by definition, do not exactly satisfy the discrete equations, and therefore, unavoidably involve certain residual errors. The matter of how small residuals must become for the numerical solution to be a

valid approximation of the governing mathematical equations is of obvious and practical relevance. In large-scale computations it may be prohibitively expensive to converge all solvers to machine precision. A popular execution mode, therefore, is for a solver to perform a fixed number of iterations and then proceed to subsequent steps in the algorithm. The ramifications of such an approach on the evolution of the solution are difficult to conjecture.

A powerful technique that can unravel this complexity and ultimately help to verify these solvers is the method of manufactured solutions (MMS). Manufactured solutions are exact solutions to a set of governing equations that have been modified with forcing terms. This concept has been around since the early days of computer codes (see, for example, Burggraf 1966) and has been more recently formalized under the name MMS in a series of papers (Roache 1998*a*,*b*, 2002; Knupp & Salari 2003; Oberkampf *et al.* 2004; Roy 2005). The objective of this work is to use the method of manufactured solutions to explore the effects of tabulated constitutive relationships and iteration errors on the computational performance of low-Mach number combustion codes.

2. Mathematical model

2.1. *Governing equations*

The simulations in this report are performed using the unstructured large-eddy simulation (LES) code CDP †. The LES methodology recognizes that in many practical simulations, the governing equations admit solutions that cannot be resolved on affordably-sized grids. A filter, denoted here by an overbar, is therefore introduced to separate the flow into resolved and unresolved scales. The large scales of motion are directly simulated while the smaller, dissipative scales are modeled. All field variables are decomposed into resolved and unresolved (or subgrid-scale) components using either a Reynolds decomposition

$$\rho = \bar{\rho} + \rho' \tag{2.1}$$

or a Favre (density-weighted) decomposition:

$$u_i = \tilde{u}_i + u_i'', \qquad \tilde{u}_i = \overline{\rho u_i}/\bar{\rho}. \tag{2.2}$$

Filtering the continuum Navier-Stokes equations yields equations for the resolved-scale variables: density $\bar{\rho}$, pressure $\bar{p}$, velocity $\tilde{u}_i$, and transported scalars $\tilde{\phi}_k$.

The combustion systems of interest in this work are characterized by relatively low Mach numbers ($Ma < 0.3$), hence, the assumption of negligible compressibility and acoustic effects is generally valid. The density is allowed to vary with the local temperature and species concentration (i.e. the transported scalars), but is not a function of the local pressure.

Under these simplifications, variable-density reacting flows are described by the following conservation equations for mass, momentum, and species, combined with a suitable EOS:

† CDP is a set of massively parallel unstructured flow solvers developed specifically for Large Eddy Simulation by Stanford's Center for Integrated Turbulence Simulations as part of the Department of Energy's ASC Alliance Program, see http://cits.stanford.edu. CDP is named after Dr. Charles David Pierce (1969-2002)

$$\frac{\partial \bar{\rho}}{\partial t} + \frac{\partial \bar{\rho}\tilde{u}_j}{\partial x_j} = \bar{\dot{S}}_{\bar{\rho}} \tag{2.3}$$

$$\frac{\partial \bar{\rho}\tilde{u}_i}{\partial t} + \frac{\partial \bar{\rho}\tilde{u}_j\tilde{u}_i}{\partial x_j} = -\frac{\partial \bar{p}}{\partial x_i} + \frac{\partial}{\partial x_j}\left(2\bar{\mu}\tilde{S}_{ij} - q_{ij}\right) + \bar{\dot{S}}_{\bar{u}_i} \tag{2.4}$$

$$\frac{\partial \bar{\rho}\tilde{\phi}_k}{\partial t} + \frac{\partial \bar{\rho}\tilde{u}_j\tilde{\phi}_k}{\partial x_j} = \frac{\partial}{\partial x_j}\left(\bar{\rho}\tilde{\alpha}_k\frac{\partial \tilde{\phi}_k}{\partial x_j} - q_{\tilde{\phi}_k j}\right) + \bar{\dot{S}}_{\tilde{\phi}_k} \tag{2.5}$$

$$\bar{\rho} = f(\tilde{\phi}_1, \tilde{\phi}_2, ...). \tag{2.6}$$

The resolved-scale stress is given by

$$\tilde{S}_{ij} = \frac{1}{2}\left(\frac{\partial \tilde{u}_i}{\partial x_j} + \frac{\partial \tilde{u}_j}{\partial x_i}\right) - \frac{1}{3}\delta_{ij}\frac{\partial \tilde{u}_k}{\partial x_k}, \tag{2.7}$$

and the subgrid (or subfilter) stress q_{ij} and scalar fluxes $q_{\tilde{\phi}_k j}$ are modeled using the eddy-viscosity approach of Smagorinsky (1963):

$$q_{ij} = -2\mu_t\tilde{S}_{ij} \qquad \text{where} \qquad \mu_t = \bar{\rho}\,C\,\Delta^2|\tilde{S}|. \tag{2.8}$$

The unknown coefficient C in Eq. 2.8 is closed using the dynamic procedure (Germano *et al.* 1991; Moin *et al.* 1991; Ghosal *et al.* 1995; Pierce & Moin 1998). In all simulations reported here, the codes are run in so-called "DNS" mode, wherein all subgrid models are disabled.

2.2. *Numerical method*

The computer code CDP uses a collocated, unstructured version of the algorithm of Pierce & Moin (2001, 2004). This algorithm employs a temporally-staggered variable arrangement in which velocity components are staggered in time with respect to density and other scalar variables. The equations are spatially discretized using low-dissipation, node-based finite-volume operators developed by Ham *et al.* (2006). The variables are implicitly advanced in time using a fractional-step method, and an iterative approach is used at each time level to repair splitting errors and enhance stability. The major features of the iteration process at each time step are listed below. Here the superscript m is used to denote the outer-iteration number.

1. The scalar equation(s) Eq. 2.5 are advanced in time. This yields $(\rho\phi)^{m+1}$, from which a provisional estimate for ϕ is obtained by $\widehat{\phi} = (\rho\phi)^{m+1}/\rho^m$.
2. The momentum equations Eq. 2.4 are advanced to obtain provisional velocities: $\widehat{u_i}$.
3. The provisional scalar values are used to evaluate the density from the EOS: $\rho^{m+1} = f(\widehat{\phi})$.
4. The updated density is used to correct the scalar(s) to ensure primary conservation: $\phi^{m+1} = (\rho\phi)^{m+1}/\rho^{m+1}$.
5. A constant-coefficient Poisson equation is solved for pressure, and the result is used to correct the velocity field to discretely conserve mass.
6. The process is repeated from step 1 and continued until convergence.

The linearized scalar and momentum equations (steps 1-2) are solved using a Jacobi method, and the Poisson solve (step 5) is accomplished using the HYPRE algebraic multigrid solver (Falgout & Yang 2002; Henson & Yang 2002). Linear analysis indicates

that the iterative approach outlined above is second-order accurate when at least two outer iterations are employed (Pierce & Moin 2001). Additional iterations may improve the stability of the scheme, but do not increase the order of accuracy. Formal verification of the second-order behavior of the algorithm requires convergence of the system at each time step.

3. Method of manufactured solutions

3.1. *Background*

The method of manufactured solutions (MMS) is a general procedure that can be used to construct analytical solutions to the differential equations that form the basis of a simulation code. The resulting solutions, while not necessarily physically relevant, can be used as benchmark solutions for verification tests. The accuracy of the code is gauged by running the test problems on systematically refined grids and comparing the output with the analytical manufactured solution. The behavior of the error is examined against the theoretical order-of-accuracy inherent in the code's numerical discretizations. Thus, a verification test using MMS provides an unambiguous result as to whether or not the algorithm is implemented correctly. MMS has been successfully applied in a variety of applications including fluid dynamics (Roy *et al.* 2004; Bond *et al.* 2006), heat transfer (Brunner 2006; Domino *et al.* 2007), fluid-structure interaction (Tremblay *et al.* 2006), even turbulence modeling (Eca *et al.* 2007).

Application of MMS is conceptually straightforward. Consider a generic system of differential equations

$$\mathsf{D}(\boldsymbol{\psi}) = 0 \tag{3.1}$$

where $\boldsymbol{\psi}$ is a vector of unknown variables and $\mathsf{D}(\cdot)$ is a differential operator whose specific form depends on the governing partial differential equations. In MMS, the analyst selects a sufficiently differentiable function $\widehat{\boldsymbol{\psi}}$ to describe the desired evolution of the variables in space and time. Since $\widehat{\boldsymbol{\psi}}$ does not necessarily satisfy the original governing equations Eq. 3.1, a corresponding set of source terms $\boldsymbol{S}_{\boldsymbol{\psi}}$ are "manufactured" by simply applying the differential operator to $\widehat{\boldsymbol{\psi}}$ in order to balance the system

$$\mathsf{D}(\widehat{\boldsymbol{\psi}}) = \boldsymbol{S}_{\boldsymbol{\psi}}. \tag{3.2}$$

The new set of equations given by Eq. 3.2 constitutes an exact analytical solution that exercises all of the same differential terms as Eq. 3.1. Consequently, Eq. 3.2 can be used to test numerical codes designed to solve Eq. 3.1 with minimal additional coding.

As the generality of the current discussion demonstrates, there is near limitless flexibility in constructing manufactured solutions. A useful set of guidelines for the effective design and application of MMS are contained in the monograph by Knupp & Salari (2003).

3.2. *Example problems*

In this section we introduce example MMS problems which attempt to illustrate "canonical" phenomena in variable-density flows. It has been argued that because code verification is a purely mathematical exercise, manufactured solutions need not be "realistic" (Roache 2002). While this statement is unquestionably true, it does not fully acknowledge the utility of well-crafted manufactured solutions in identifying the vulnerabilities and strengths of a computational algorithm. For instance, a manufactured solution that

is *suggestive* of some elementary physics, provides not only a statement about the code's order-of-accuracy, but also gives a preview of how the code might perform in more complex problems where the mimicked physics are pervasive.

In this spirit, the current examples are constructed such that they identically obey a subset of the governing physics without extra source terms (for example, they analytically conserve mass), and apply manufactured sources to satisfy the remaining conservation laws. Mass conservation is afforded preferential treatment in these examples due to its central role in the solution algorithm presented in Section 2.2. The resulting manufactured solutions attempt to balance simplicity with realism in an effort to understand how the code performs in "representative" scenarios.

The verification problems in this report are based on the EOS for isothermal binary mixing between miscible fluids:

$$\rho(\phi) = \left(\frac{\phi}{\rho_1} + \frac{1-\phi}{\rho_0} \right)^{-1}. \tag{3.3}$$

Although this EOS is simple, it is deceptively nontrivial. Large density ratios result in extremely non-linear behavior that can challenge variable-density solvers in a manner similar to the reactive state-equations associated with combustion chemistry. The scalar variable ϕ in Eq. 3.3 is known as the mixture fraction and assumes values ranging from 0 to 1. A similar mixture fraction variable is ubiquitously used in combustion modeling to describe the "mixedness" between fuel and oxidizer. The quantities ρ_0 and ρ_1 are the pure component densities, i.e. $\rho_0 = \rho(\phi = 0)$ and $\rho_1 = \rho(\phi = 1)$.

The first example problem is a one-dimensional manufactured solution reflective of binary diffusive mixing:

$$\begin{aligned}
\phi(x,t) &= \frac{\exp(-k_1 t) - \cosh(w_0 x \exp(-k_2 t))}{\exp(-k_1 t)\left(1 - \frac{\rho_0}{\rho_1}\right) - \cosh(w_0 x \exp(-k_2 t))} \\
\rho(x,t) &= \left(\frac{\phi(x,t)}{\rho_1} + \frac{1-\phi(x,t)}{\rho_0} \right)^{-1} \\
u(x,t) &= 2k_2 \exp(-k_1 t) \frac{\rho_0 - \rho_1}{\rho(x,t)} \left(\frac{\widehat{u} x}{\widehat{u}^2 + 1} + \frac{(\frac{k_1}{k_2} - 1)(\arctan \widehat{u} - \frac{\pi}{4})}{w_0 \exp(-k_2 t)} \right)
\end{aligned} \tag{3.4}$$

where $\widehat{u} = \exp(w_0 x \exp(-k_2 t))$ and w_0, k_1, and k_2 are constant parameters. Note that Eq. 3.4 satisfies the continuous continuity equation Eq. 2.3 with $\bar{\dot{S}}_{\bar{\rho}} = 0$, but produces a non-zero source term in the scalar transport equation Eq. 2.5. No source term is specified in the momentum equation, instead the pressure is allowed to compensate to satisfy Eq. 2.4 with $\bar{\dot{S}}_{\tilde{u}_i} = 0$. If interested, one could solve for the analytical pressure distribution by integrating Eq. 2.4 with respect to x. The relevant manufactured scalar source term is computed by substituting Eq. 3.4 into Eq. 2.5 and solving for $\bar{\dot{S}}_{\tilde{\phi}_k}$. The spatio-temporal evolution of Eq. 3.4 is shown in Fig. 1 for the parameter values in Table 1. The computational domain for this problem is $0 \leq x \leq 2$ and $0 \leq t \leq 1$. A similar problem was investigated by Shunn & Ham (2006), although not within the framework of MMS.

A second MMS problem involves a two-dimensional corrugated front with advection and diffusion:

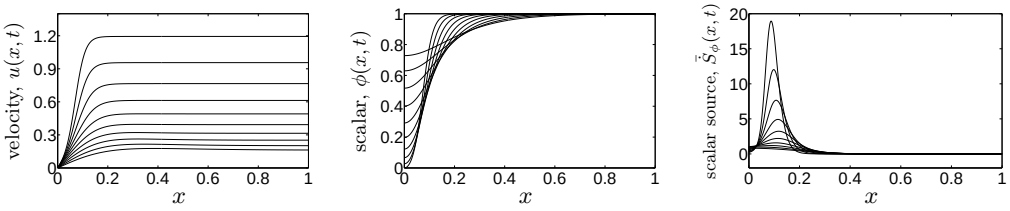

FIGURE 1. 1-D manufactured solution. (left to right) $u(x,t)$, $\phi(x,t)$, $\bar{\dot{S}}_\phi(x,t)$.

TABLE 1. Parameter values for 1-D problem.

parameter	value
ρ_0	20
ρ_1	1
k_1	4
k_2	2
w_0	50
$\bar{\rho}\tilde{\alpha}_\phi = \bar{\mu}$	0.03

TABLE 2. Parameter values for 2-D problem.

parameter	value	parameter	value
ρ_0	20	a	1/5
ρ_1	1	b	20
u_f	1	k	4π
v_f	1/2	ω	3/2
$\bar{\rho}\tilde{\alpha}_\phi$	0.001	$\bar{\mu}$	0.001

$$
\begin{aligned}
\phi(x,y,t) &= \frac{1+\tanh(b\widehat{x}\exp(-\omega t))}{(1+\frac{\rho_0}{\rho_1})+(1-\frac{\rho_0}{\rho_1})\tanh(b\widehat{x}\exp(-\omega t))} \\
\rho(x,y,t) &= \left(\frac{\phi(x,y,t)}{\rho_1}+\frac{1-\phi(x,y,t)}{\rho_0}\right)^{-1} \\
u(x,y,t) &= \frac{\rho_1-\rho_0}{\rho(x,y,t)}\Bigg(-\omega\widehat{x}+\frac{\omega\widehat{x}-u_f}{\exp(2b\widehat{x}\exp(-\omega t))+1} \\
&\qquad\qquad +\frac{\omega\log(\exp(2b\widehat{x}\exp(-\omega t))+1)}{2b\exp(-\omega t)}\Bigg) \\
v(x,y,t) &= v_f \\
p(x,y,t) &= 0
\end{aligned}
\tag{3.5}
$$

where $\widehat{x}(x,y,t) = u_f t - x + a\cos(k(v_f t - y))$ and a, b, k, ω, u_f, and v_f are constant parameters. Eq. 3.5 satisfies the continuous continuity equation Eq. 2.3 with $\bar{\dot{S}}_{\bar{\rho}} = 0$. Non-zero source terms appear in the x and y momentum equations Eq. 2.4 and the scalar transport equation Eq. 2.5. The evolution of the density field described by Eq. 3.5 is shown in Fig. 2 given the parameter values in Table 2. The computational domain for this problem is $-1 \leq x \leq 3$, $-1/2 \leq y \leq 1/2$, and $0 \leq t \leq 1$.

In order to focus on the effects of density, the viscosity $\bar{\mu}$ and the "dynamic" diffusivity $\bar{\rho}\tilde{\alpha}_k$ in Eqs. 2.4 and 2.5 are assumed constant in both the one- and two-dimensional MMS examples.

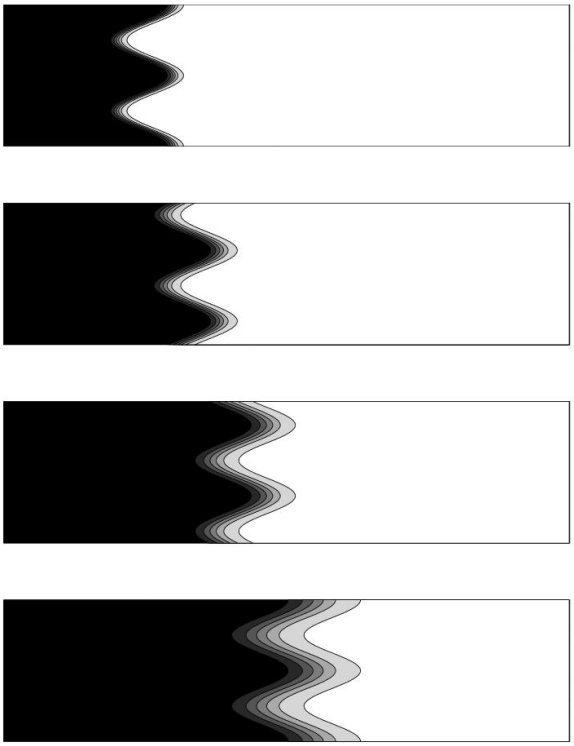

FIGURE 2. 2-D manufactured solution: $\rho(x, y, t)$ (top to bottom) $t = 0$, $t = 1/3$, $t = 2/3$, $t = 1$. (black: $\rho = 1$, white: $\rho = 20$).

4. Results

A spatial grid-refinement study using the one-dimensional example problem Eq. 3.4 was conducted to assess the convergence properties of CDP's numerics. Computational grids consisting of 64, 128, 256, 512, 1024, and 2048 control volumes were used. A time step of $\Delta t = 0.00125$ was applied in all cases, leading to maximum CFL numbers in the range 0.048 to 1.53. The boundary conditions at $x = 0$ were $u = 0$ and $\partial\phi/\partial x = 0$. An "outlet" boundary condition was applied at $x = 2$, a location sufficiently removed from the problem dynamics so as to not to introduce significant errors in the solution. The velocity, pressure, and scalar values were solved from Eqs. 2.3-2.5, and the density was evaluated using the analytical function Eq. 3.3 and the instantaneous scalar field. The convergence tolerance for solving transport equations and the pressure Poisson equation was 1×10^{-8}. Outer iterations at each time step were continued until the maximum density difference between iterations $|\rho^{m+1} - \rho^m|$ was less than 1×10^{-8}. This was typically achieved after 20–25 outer iterations. Additional problem parameters are listed in Table 1.

The maximum error (L_∞-error) and volume-averaged (L_2-error) for $u(x, t)$, $\phi(x, t)$, and $\rho(x, t)$ were monitored throughout the simulation. The error trends toward second-order convergence with respect to Δx for all variables, as seen in Fig. 3. Detailed convergence results of the exercise are tabulated in Table 3. Plots of the L_2-error versus time for $u(x, t)$ and $\phi(x, t)$ are shown in Figs. 4 and 5. Note that the error smoothly decays with

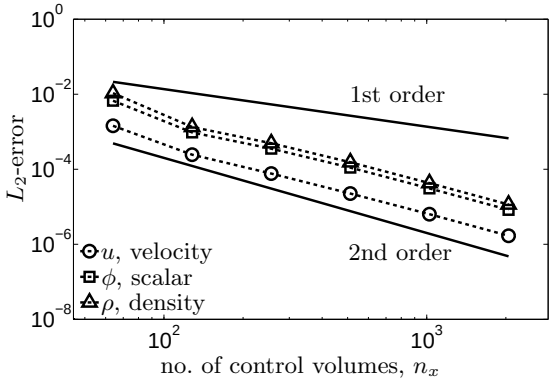

FIGURE 3. 1-D manufactured solution: L_2-error at t=1.

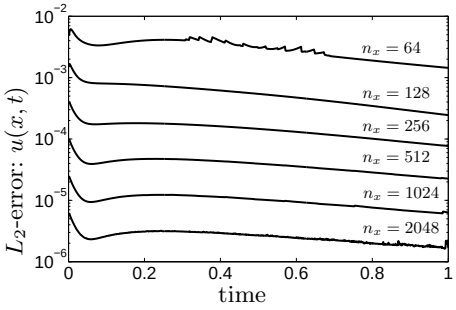

FIGURE 4. L_2-error in velocity $u(x,t)$ versus time for 1-D manufactured solution.

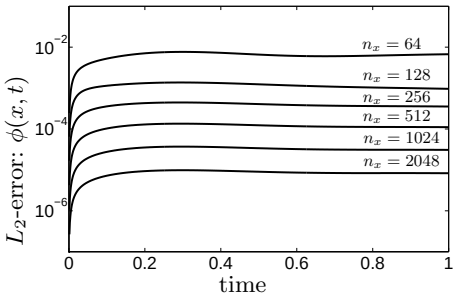

FIGURE 5. L_2-error in scalar $\phi(x,t)$ versus time for 1-D manufactured solution.

time in each simulation as the flow features diffuse and become more easily resolved. The L_∞-error behaves similarly on all grids except the $n_x = 2048$ grid, where iteration and time errors begin to contaminate the solution after $t \geq 0.5$. As part of a separate temporal-refinement study (not shown here) the time step was halved to $\Delta t = 0.000625$ and the simulations were repeated on the $n_x = 1024$ grid. The results were almost indistinguishable, with a maximum difference on the order of 10^{-6} for all variables. This suggests that the results are "converged" in a temporal sense, and that time errors are subservient to spatial errors on all of the grids with $n_x \leq 1024$.

In order to evaluate the effect of EOS tabulation on code performance, a refinement study was conducted in which the EOS Eq. 3.3 was interpolated linearly from successively-refined tables of uniformly-spaced points in ϕ-space. A summary of the tabulation resolutions and their associated errors is found in Table 4. Interpolation of the EOS at the coarsest resolutions in Table 4 would not be unreasonable in many engineering calculations where property tables are multi-dimensional (typically 3–4) and memory is limited.

The simulations were effected on a grid of 1024 control volumes with a time step of $\Delta t = 0.00125$. The boundary conditions and solver convergence limits were identical to the spatial grid-refinement study above. The full convergence results are tabulated in Table 5, and plots of the temporal evolution of the L_2-error for $u(x,t)$ and $\phi(x,t)$ are shown in Figs. 6 and 7. The "$n_\phi = \infty$" label indicates results using the analytical or non-interpolated EOS.

TABLE 3. 1-D manufactured solution: L_∞- and L_2-error at t=1 versus spatial grid refinement.

no. of points	L_∞-error $u(x,t)$	observed order	L_2-error $u(x,t)$	observed order	L_∞-error $\phi(x,t)$	observed order	L_2-error $\phi(x,t)$	observed order
64	4.5418e-03		1.4409e-03		2.6407e-02		6.7197e-03	
128	7.9587e-04	2.51	2.4485e-04	2.56	3.2633e-03	3.02	9.5846e-04	2.81
256	2.3931e-04	1.73	7.6850e-05	1.67	1.1724e-03	1.48	3.5391e-04	1.44
512	6.7858e-05	1.82	2.2545e-05	1.77	3.5933e-04	1.71	1.1075e-04	1.68
1024	1.8171e-05	1.90	6.3385e-06	1.83	9.9106e-05	1.86	3.0840e-05	1.84
2048	1.0434e-05	0.80	1.6845e-06	1.91	2.6574e-05	1.90	8.2872e-06	1.90

TABLE 4. EOS look-up table: resolutions and errors.

no. of points	max error $\rho(\phi)$	avg error $\rho(\phi)$
21	1.6118e+00	7.3605e-02
31	9.4647e-01	3.3885e-02
51	4.4249e-01	1.2463e-02
101	1.3878e-01	3.1475e-03
201	3.9362e-02	7.8898e-04
401	1.0521e-02	1.9738e-04
801	2.7226e-03	4.9353e-05

The data clearly indicate a degradation of accuracy when using a tabulated EOS. Velocity convergence inclines towards first-order behavior, while scalar and density convergence appears to be closer to second-order (with respect to $\Delta\phi$). These trends, however, are speculative at best as the data are not well converged, even with 801 interpolation points in the EOS. It is likely that convergence of the scalar outperforms velocity because of the manufactured source term in Eq. 2.5. In the simulations, the scalar source was evaluated as a function of x and t, rather than $u(x,t)$, $\phi(x,t)$, and $\rho(x,t)$. The source term, therefore, implicitly used the analytical EOS and was partially shielded from the influence of tabulation errors. It is not surprising, therefore, that scalar convergence was less affected than velocity, especially when considering the relative strength of the scalar source term in this example (see Fig. 1).

In addition to poor convergence rates, it is clear that EOS interpolation dramatically affects the character of the error in the field variables. The smooth error decay exhibited in Fig. 4 is replaced by the unsteadiness apparent in Fig. 6. These numerical fluctuations result from the tight coupling between density, velocity, and pressure in low-Mach number projection methods. Density errors arising from the tabulation are readily translated into velocity errors as the pressure acts to "correct" changes in the global mass-balance. The velocity and density in turn influence the evolution of the scalar field in a non-

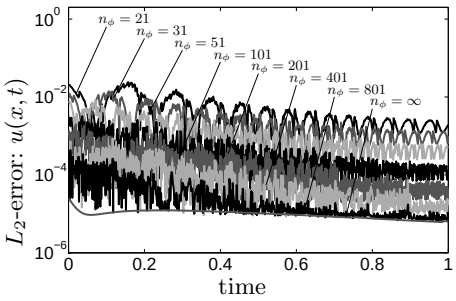

FIGURE 6. L_2-error in velocity $u(x,t)$ versus time for 1-D manufactured solution on $n_x = 1024$ grid.

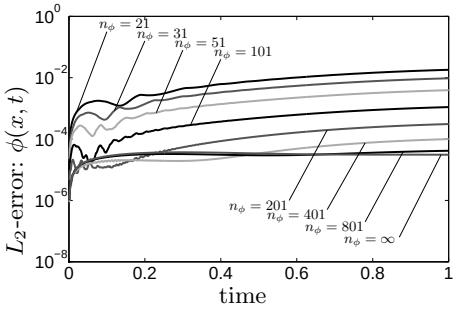

FIGURE 7. L_2-error in scalar $\phi(x,t)$ versus time for 1-D manufactured solution on $n_x = 1024$ grid.

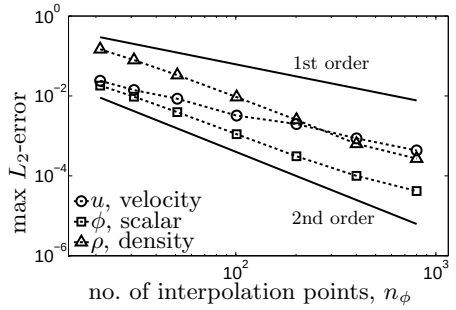

FIGURE 8. 1-D manufactured solution: convergence of maximum L_2-error on $n_x = 1024$ grid.

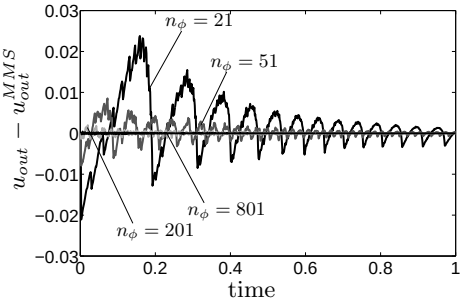

FIGURE 9. 1-D manufactured solution: convective outlet velocity $u(x = 2, t)$ on $n_x = 1024$ grid.

linear manner, adding further complexity. The end result is that small errors in the EOS evaluation can amplify and produce relatively large errors in the velocity and scalar fields.

The numerical fluctuations induced by EOS interpolation errors undoubtedly find expression in the flow variables on a macro-scale. This is readily visible in Fig. 9, which shows the convective outlet velocity $u(x = 2, t)$ for different EOS resolutions. Here, interpolation errors cause dramatic fluctuations about the exact MMS value. The presence of these fluctuations, whose genesis is entirely numerical, holds serious implications for subgrid modeling of combustion and turbulence phenomena.

Issues relating to time-accuracy and the error-contribution from iteration residuals have also been studied using MMS. Here the two-dimensional problem (Eq. 3.5) was simulated on computational grids of 200×50, 400×100, 800×200, and 1600×400 hexahedral control volumes with a uniform time step of $\Delta t = 0.00125$. This time step produced maximum CFL numbers ranging from 0.15 to 1.18 on the various grids. Dirichlet boundary conditions were imposed at $x = -1$, an "outlet" boundary condition was applied at $x = 3$, and periodic boundary conditions were used at $y = \pm 1/2$. Tolerances for the scalar, momentum, and pressure solvers were set to 1×10^{-10} in all simulations. Additional problem parameters are supplied in Table 2.

A major focus of this study was to investigate the effect of applying multiple non-linear iterations to "fully" converge the system of equations at each time step. Fig. 10 shows the spatial-convergence of the L_2-error of the flow variables when 20 outer iterations are employed. At this level of iteration, the bulk of the time error is eliminated and

TABLE 5. 1-D manufactured solution: maximum L_∞- and L_2-error versus EOS look-up table refinement.

no. of points	L_∞-error $u(x,t)$	observed order	L_2-error $u(x,t)$	observed order	L_∞-error $\phi(x,t)$	observed order	L_2-error $\phi(x,t)$	observed order
21	3.0450e-02		2.3991e-02		5.4061e-02		1.8100e-02	
31	1.8274e-02	1.31	1.4032e-02	1.38	2.8370e-02	1.66	9.5723e-03	1.64
51	9.2087e-03	1.38	8.5121e-03	1.00	1.1613e-02	1.79	3.9251e-03	1.79
101	3.5173e-03	1.41	3.2208e-03	1.42	3.2998e-03	1.84	1.1030e-03	1.86
201	2.0185e-03	0.81	1.9794e-03	0.71	9.6504e-04	1.79	3.0885e-04	1.85
401	9.2466e-04	1.13	8.6672e-04	1.20	3.4493e-04	1.49	9.9923e-05	1.63
801	5.2006e-04	0.83	4.3319e-04	1.00	1.5400e-04	1.17	4.1577e-05	1.27

all variables trend toward second-order convergence with grid refinement — confirming the expected accuracy of CDP's spatial operators. Fig. 11 shows how the convergence is affected when fewer outer iterations are used at each time level. The observed convergence is approximately first-order when 10 iterations are applied, and even less promising with fewer iterations.

The errors depicted in Fig. 11 are a combination of spatial and temporal contributions that combine in a complex manner on different grids and time steps. A closer examination of the temporal component of the error is instructive. Fig. 12 shows the convergence of the L_2-error with respect to Δt for a simulation on the 800×200 grid and applying only one outer iteration per time step. Details of the modifications to the time advancement required to avoid outer iterations are presented elsewhere in this volume (Ham 2007). Under these conditions, the dominant error derives from the time advancement which is clearly first-order accurate. Additional outer iterations help to repair the time-errors either increasing their accuracy towards second-order and/or reducing their magnitude.

In a related study, the simulations of Fig. 11 were repeated using a more moderate density ratio of $\rho_0/\rho_1 = 5$. In this case, second-order convergence was observed after 5–10 outer iterations versus the 15–20 iterations for the $\rho_0/\rho_1 = 20$ case. This accelerated convergence is encouraging for applications with modest density ratios, but also indicates an unappealing dependence of the algorithm's convergence properties on the EOS.

5. Conclusions and future work

In this study, the method of manufactured solutions (MMS) was used to investigate the effects of tabulated state-equations and temporal iteration errors on the convergence and accuracy of the multi-physics hydrodynamics code CDP. Two MMS problems were constructed whose evolution is reflective of some of the basic physics germane to combustion problems, namely: diffusive mixing of species and convection of density fronts. Both of the MMS examples analytically satisfy the source-free continuity equation, and use manufactured source terms to balance other transport equations in the system. Grid refinement studies performed using the MMS problems confirm the spatial convergence rate of CDP to be second-order when an analytical EOS is used. Convergence of the flow variables to the exact solution was markedly impaired when the EOS was linearly

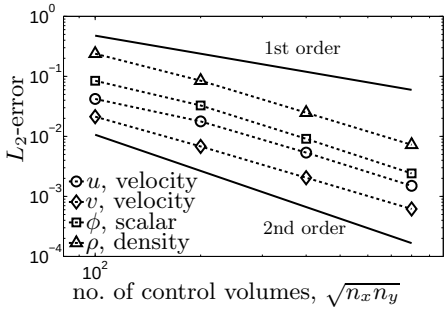

FIGURE 10. 2-D manufactured solution: L_2-error at $t = 1$ using 20 outer iterations.

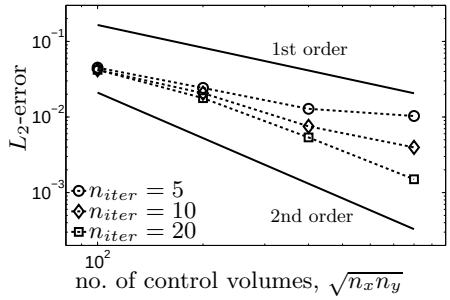

FIGURE 11. 2-D manufactured solution: L_2-error of $u(x,t)$ at $t = 1$ for different numbers of outer iterations.

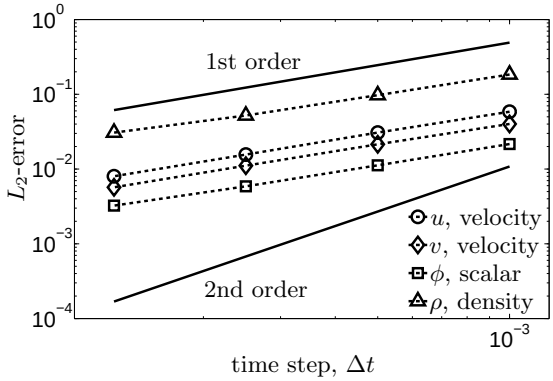

FIGURE 12. 2-D manufactured solution: L_2-error at t=0.1 using 1 outer iteration.

interpolated in ϕ-space. EOS interpolation errors introduce spurious numerical fluctuations in the flow variables, with velocity and pressure being particularly vulnerable. In some problems these errors can accumulate with time and potentially alter the temporal evolution of the flow. The variable density algorithm in CDP has first-order temporal accuracy when a single outer iteration is applied. Temporal errors were generally not dominant when multiple outer iterations were performed, making it difficult to confirm the temporal accuracy of the method with multiple outer iterations.

The present results suggest that, for a given problem, a balance exists between factors such as the size of the time step and the number of outer iterations that need to be performed. Determining the optimal operating conditions (i.e. grid size, time step, number of outer iterations, etc.) is a nontrivial and problem-dependent task that deserves more attention than is currently afforded. Future work will include the development of a more complete test suite of MMS problems suitable for variable-density solvers and their application to other low-Mach number combustion codes.

Acknowledgments

This work was supported by the U.S. Department of Energy through the Advanced Simulation and Computing (ASC) program.

REFERENCES

Bond, R. B., Ober, C. C. & Knupp, P. M. 2006 A manufactured solution for verifying CFD boundary conditions, part III. In *36th AIAA Fluid Dynamics Conference*, vol. 3, pp. 1966–1982. San Francisco, CA.

Brunner, T. A. 2006 Development of a grey nonlinear thermal radiation diffusion verification problem. *Transactions of the American Nuclear Society* **95**, 876–878.

Burggraf, O. R. 1966 Analytical and numerical studies of the structure of steady separated flows. *J. Fluid Mech.* **24**, 113–151.

Domino, S. P., Wagner, G., Luketa-Hanlin, A., Black, A. & Sutherland, J. 2007 Verification for multi-mechanics applications. In *48th AIAA/ASME/ASCE/AHS/ASC Structures, Structural Dynamics, and Materials Conference*. Honolulu, HI.

Eca, L., Hoekstra, M., Hay, A. & Pelletier, D. 2007 On the construction of manufactured solutions for one- and two-equation eddy-viscosity models. *Int. J. Num. Meth. Fluids* **54** (2), 119–154.

Falgout, R. D. & Yang, U. M. 2002 HYPRE: a library of high performance preconditioners. In *Computational Science - ICCS 2002 Part III* (ed. P. M. A. Sloot, C. J. K. Tan, J. J. Dongarra & A. G. Hoekstra), *Lecture Notes in Computer Science*, vol. 2331, pp. 632–641. Springer-Verlag.

Germano, M., Piomelli, U., Moin, P. & Cabot, W. H. 1991 A dynamic subgrid-scale eddy viscosity model. *Phys. Fluids A* **3**, 1760–1765.

Ghosal, S., Lund, T. S., Moin, P. & Akselvoll, K. 1995 A dynamic localization model for large-eddy simulation of turbulent flows. *J. Fluid Mech.* **286**, 229–255.

Ham, F. 2007 An efficient scheme for large eddy simulation of low-mach combustion in complex configurations. *Annual Research Briefs 2007* Center for Turbulence Research, Stanford University, NASA Ames.

Ham, F., Mattsson, K. & Iaccarino, G. 2006 Accurate and stable finite volume operators for unstructured flow solvers. *Annual Research Briefs 2006* Center for Turbulence Research, Stanford University, NASA Ames, 243–261.

Henson, V. E. & Yang, U. M. 2002 BoomerAMG: a parallel algebraic multigrid solver and preconditioner. *Appl. Num. Math.* **41**, 155–177.

Klimenko, A. Y. & Bilger, R. W. 1999 Conditional moment closure for turbulent combustion. *Prog. Energy Combust. Sci.* **25**, 595–687.

Knupp, P. & Salari, K. 2003 *Verification of Computer Codes in Computational Science and Engineering*. Boca Raton: Chapman & Hall/CRC.

Moin, P., Squires, K., Cabot, W. & Lee, S. 1991 A dynamic subgrid-scale model for compressible turbulence and scalar transport. *Phys. Fluids A* **3**, 2746–2757.

Oberkampf, W. L., Trucano, T. G. & Hirsch, C. 2004 Verification, validation, and predictive capability in computational engineering and physics. *Appl. Mech. Rev.* **57** (5), 345–384.

Peters, N. 1984 Laminar diffusion flamelet models in non-premixed turbulent combustion. *Prog. Energy Combust. Sci.* **10**, 319–339.

Peters, N. 2000 *Turbulent Combustion*. Cambridge: Cambridge University Press.

Pierce, C. D. & Moin, P. 1998 A dynamic model for subgrid-scale variance and dissipation rate of a conserved scalar. *Phys. Fluids* **10**, 3041–3044.

Pierce, C. D. & Moin, P. 2001 Progress-variable approach for large-eddy simulation of turbulent combustion. PhD thesis, Stanford University.

Pierce, C. D. & Moin, P. 2004 Progress-variable approach for large-eddy simulation of non-premixed turbulent combustion. *J. Fluid Mech.* **504**, 73–97.

Pope, S. B. 1985 PDF methods in turbulent reactive flows. *Prog. Energy Combust. Sci.* **11**, 119–192.

Roache, P. J. 1998*a* *Verification and Validation in Computational Science and Engineering*. Albuquerque: Hermosa Publishers.

Roache, P. J. 1998*b* Verification of codes and calculations. *AIAA Journal* **36** (5), 696–702.

Roache, P. J. 2002 Code verification by the method of manufactured solutions. *J. Fluids Eng.* **124** (1), 4–10.

Roy, C. J. 2005 Review of code and solution verification procedures for computational simulation. *J. Comp. Phys.* **205** (1), 131–156.

Roy, C. J., Nelson, C. C., Smith, T. M. & Ober, C. C. 2004 Verification of Euler/Navier-Stokes codes using the method of manufactured solutions. *Int. J. Num. Meth. Fluids* **44** (6), 599–620.

Shunn, L. & Ham, F. 2006 Consistent and accurate state evaluations in variable-density flow simulations. *Annual Research Briefs 2006* Center for Turbulence Research, Stanford University, NASA Ames, 135–147.

Smagorinsky, J. 1963 General circulation experiments with the primitive equations. *Mon. Weather Rev.* **91** (3), 99–164.

Tremblay, D., Etienne, S. & Pelletier, D. 2006 Code verification and the method of manufactured solutions for fluid-structure interaction problems. In *36th AIAA Fluid Dynamics Conference*, vol. 2, pp. 882–892. San Francisco, CA.